Journal of Inorganic and Organometallic Polymers and Materials (2020) 30:965–975
https://doi.org/10.1007/s10904-019-01227-8

Coordination Polymer Based on Nickel(II) Maleate and 4′-Phenyl-2,2′:6′,2″-Terpyridine: Synthesis, Crystal Structure and Conjugated Thermolysis

Igor E. Uflyand[1] · Vladimir A. Zhinzhilo[1] · Gulzhian I. Dzhardimalieva[2]

Received: 30 April 2019 / Accepted: 9 June 2019 / Published online: 13 June 2019

Abstract
New complex (1) based on nickel(II) maleate and 4′-phenyl-2,2′:6′,2″-terpyridine (L) was synthesized. The complex 1 is a 1D coordination polymer formed from a L-Ni(II) node bridged by maleate ligands and crystallizes in monoclinic form with space group $P2_1/n$. There are two Ni(II) moiety's in the asymmetric unit. Each nickel atom is five coordination and is chelated by three nitrogen atoms of **L** and two oxygen atoms of Mal fragments with the formation of a NiN_3O_2 chelate node. The polyhedron of the first Ni(II) moiety is close to the ideal tetragonal pyramidal structure, while the polyhedron of the second Ni(II) moiety belongs to the distorted tetragonal pyramidal structure. The main stages and kinetics features of the conjugated thermolysis of complex 1 were evaluated. Metal–polymer nanocomposite containing Ni nanoparticles uniformly distributed in a stabilizing nitrogen-containing polymer matrix was obtained.

Keywords Coordination polymer · Crystal structure · Metal chelate · Nanomaterial · Thermolysis

1 Introduction

In recent years, considerable attention of researchers has been attracted to coordination polymers containing metal chelate units, which are widely used as precursors of nanocomposite materials [1]. Among such compounds, a special place is occupied by coordination polymers, including unsaturated bonds capable of entering into polymerization transformations. The presence of two carboxylate groups in dicarboxylic acid molecules expands their ligand capabilities and allows them to create a wide range of monomeric and polymeric architectures. As a typical example, mention should be made of coordination polymers based on maleate (Mal) of transition metals, in which maleic acid can act as a mono-, bi-, and tetradentate ligand [2–13]. In particular, we found that normal Ni(II) $[Ni(Mal)(H_2O)_2](H_2O)$ maleate crystals belong to the monoclinic crystal system and both maleic acid carboxylate groups are involved in the binding of metals to form a seven-membered chelate ring [14]. At the same time, nickel bimaleate has a monomeric chain structure, in which maleic acid is a monodentate ligand [15].

The conjugated thermolysis of such compounds, including the simultaneous thermal polymerization of the starting monomer and the thermolysis of the resulting metallopolymers, leads to advanced materials based on nanoparticles of metals, their oxides or carbides stabilized by the polymer matrix [16]. For example, four types of nanoparticles were found in the products of conjugated thermolysis of cobalt(II) maleate: α-Co, β-Co, and CoO (2–12 nm) in polymer shells and Co_3O_4 without a polymer shell [13]. At the same time, the conjugated thermolysis of nickel maleates led to nanoparticles of metallic nickel (4–5 nm) coated with two to five layers of graphene [10]. Note also that the products of thermolysis of iron(III) and copper(II) maleates are Fe_3O_4 nanoparticles (4–9 nm) and copper aggregates ranging in size from 50 nm to several microns [7]. It is important that the composition and structure of products of conjugated thermolysis are determined by the conditions of thermolysis (temperature, gaseous medium), the ligand environment, and the nature of the metal. In addition, data on the phase

✉ Igor E. Uflyand
ieuflyand@sfedu.ru

[1] Department of Chemistry, Southern Federal University, Rostov-on-Don, Russian Federation 344006

[2] Laboratory of Metallopolymers, The Institute of Problems of Chemical Physics RAS, Chernogolovka, Moscow Region, Russian Federation 344006

composition of the resulting nanomaterials make it possible to predict their functional properties [17].

One of the promising areas of research for unsaturated metal carboxylates is to obtain mixed-ligand complexes, including unsaturated carboxylic acids and polypyridine ligands, for example, 1,10-phenanthroline (phen) [18, 19], 2,2′-bipyridine (bpy) [20], and others. Such complexes are characterized by a wide variety of compositions and spatial architectures of the formed compounds. In particular, various types of complexes $[Ni(Mal)(bpy)(H_2O)_3]\cdot H_2O$, $[Ni(Mal)(bpy)_2]0.7\cdot 34H_2O$ and $[Ni(Mal)(bpy)(H_2O)_3]H_2O$ were obtained on the basis of nickel maleate and bpy [21–23]. At the same time, the interaction of nickel(II) maleate and phen in different reaction conditions made it possible to obtain $[Ni(Mal)(phen)(H_2O)_3]\cdot 2H_2O$ [24], $[Ni(Mal)(phen)(H_2O)_3]\cdot H_2O$, $[Ni(Mal(phen)(H_2O)_2]\cdot 2H_2O$ complexes [25]. Depending on the conditions of conjugated thermolysis of mixed-ligand complexes, nanoparticles of metal oxide or pure metal were obtained, uniformly distributed in a stabilizing nitrogen-containing polymer matrix [26] However, a detailed study of the kinetics of thermal transformations of such complexes has not yet been carried out.

In the past decades, coordination complexes based on substituted 2,2′:6′,2″-terpyridine have been widely investigated for their diverse structures [27–32] and potential applications in luminescence [33–37], magnetism [38–41], sensing [42, 43], catalysis [44–46], organic light emitting diodes [47] and redox and photophysical properties [48]. It is of interest to use metal complexes with vinyl-derived terpyridines as metal-containing monomers [49–53]. To our knowledge, the complexes of unsaturated metal dicarboxylates with terpyridine derivatives have not been practically studied. Here we report on the synthesis, characterization and thermal properties of new complex (**1**) based on nickel(II) maleate [Ni(Mal)] and 4′-phenyl-2,2′:6′,2″-terpyridine (**L**). This paper is a continuation of our studies on thermal transformations of unsaturated nickel(II) carboxylates and the properties of the resulting nanocomposites [2–4, 14, 17].

2 Experimental

2.1 Reagents

All reagents were purchased from Aldrich and Merck and used without further purification.

Nickel(II) maleate was synthesized according to the following method. To 2.32 g maleic acid (0.1 mol) dissolved in 20 cm^3 H_2O 2.38 g freshly prepared nickel basic carbonate (0.1 mol) were introduced. The mixture was stirred until gas evolution stops and heated in a water bath at 60 °C until a green crystalline precipitate was formed. Without allowing to cool, the precipitate is separated on a porous glass plate, washed with a small amount of ice water and dried first in air and then in vacuum at 40 °C. Yield is 1.36 g (61.26% based on maleic acid). The resulting compound corresponds to the hydrated nickel bimaleate $Ni(C_8H_6O_8)\cdot 4H_2O$. Found (%): C 26.87; H 4.0; Ni 16.44. $C_8H_{14}O_{12}Ni$. Calcd (%): C 26.6; H 3.88; Ni 16.34. IR (KBr pellet), ν/cm^{-1}: 3540 and 3400 (O–H); 3043 ν(=C–H); 1649 ν(C=C); 1620 $\nu(H_2O)$; 1578 and 1442 ν_{as}(C=O); 1067 (=CH–C); 1547, 1524 ν_s(C=O).

The complex (**1**) of nickel(II) maleate with 4′-phenyl-2,2′:6′,2″-terpyridine (**L**) was synthesized as follows. To 3.61 g nickel bimaleate tetrahydrate (0.01 mol) dispersed in 30 mm^3 of ethanol a suspension of 3.09 g **L** (0.01 mol) in 20 mm^3 of ethanol was gradually added stirring on a magnetic stirrer. After making the entire amount of **L**, the mixture is stirred for 30 min and heated at 50 °C for 1.5 h. The hot mixture is quickly filtered through a porous glass plate and left in a tightly closed vessel at room temperature. Within 3–5 days, the product crystallizes in the form of light-green monoclinic crystals. The crystals are separated by filtration under vacuum on a glass plate, quickly washed with a small amount of ethanol and dried in vacuum at 40 °C. Yield is 3.64 g (60.87%). Found (%): C, 62.21; H, 3.5; N, 8.6; Ni, 12.84. $C_{50}H_{34}O_8N_6Ni_2$. Calcd (%): C, 62.24; H, 3.53; N, 8.71; Ni, 12.24. IR (KBr pellet), ν/cm^{-1}: 3408 and 3387 (O–H); 3043 ν(=C–H), 1644 (C=C); 1620 (heterocycle); 1583 and 1427 ν_{as}(C=O), 1520, 1384 ν_s(COO); 1106 (=CH–C).

2.2 Characterization

Elemental analyses were carried out on a CHNOS vario EL cube analyzer (Elementar Analysensysteme GmbH, Germany), their results were found to be in good agreement (±0.3%) with the calculated values. Nickel was determined on an energy dispersive X-ray fluorescence spectrometer «X-Art M» (Comita, Russian) or atomic absorption spectrometer «MGA-915» (Lumex, Russia). IR spectra were performed on the Perkin-Elmer Spectrum 100 FTIR spectrometer using KBr tablets and Softspectra data analysis software. Thermal analysis and differential scanning calorimetry were carried out on synchronous thermal analyzer STA 409CLuxx coupled to quadrupole mass spectrometer QMS 403CAeolos (NETZSCH, Germany) and on a Perkin-Elmer Diamond TG/DTA derivatograph under air (powders, m = 0.3–0.4 g) with the standard α-Al_2O_3 at a rate of 10 K/min in the range of 20–800 °C. X-ray diffraction analysis was carried out on the diffractometer DRON-UM-2 with CuKα radiation (λCu = 1.54184 Å) in the range of 2θ = 5–80° angles 2θ with a scan rate of 50/min and a temperature of 25 °C to determine the phase composition and the size of the crystallites. The size of crystallites of nanomaterials (D, nm) was determined by the Debye–Scherrer equation:

$$D = \frac{K \cdot \lambda}{\beta \cos\theta}, \quad (1)$$

where K is a constant (ca. 0.9); λ is the X-ray wavelength used in XRD (1.5418 Å); θ is the Bragg angle; β is the pure diffraction broadening of the peak at half-height that is, broadening due to the crystallite size.

The structure of metal–polymer nanocomposites was studied with a Tecnai G2 Spirit BioTWIN FEI high-resolution transmission microscope (Netherlands). Samples for transmission electron microscopy were prepared as follows: a powder suspension in hexane was applied onto a carbon-coated copper grid and the solvent was dried in air.

2.3 Study of the Thermolysis Kinetics

The kinetics of the isothermal transformations of complex **1** was studied based on gas evolution in static nonisothermal reactor using a membrane zero manometer (Fig. 1). Thermolysis was carried out under static isothermal conditions at temperatures T_{exp} in an argon atmosphere. The weight loss of the sample (Δm, wt%) and the amounts of gaseous products at ~ 20 °C were determined at the end of the experiments. The volume of the heated tube did not exceed 0.05 V, where V is the total reactor volume. The ratio $m_0/V = (0.60–3.85) \times 10^{-3}$ g cm^{-3}, where m_0 is the initial weight of the sample.

2.4 X-Ray Crystallography

X-ray structure analysis of a single crystal of complex **1** was conducted on a Bruker SMART APEX II diffractometer equipped with a CCD detector (MoKα-radiation, λ = 0.71073 Å, graphite monochromator). The intensity data were collected and integrated using the Bruker APEX2 and SMART software suites. A semiempirical absorption correction was applied [64]. The structure was solved by direct methods and refined by full-matrix least squares in the anisotropic approximation for all non-hydrogen atoms. All hydrogen atoms were placed in calculated positions and were refined isotropically in the riding model with $U_{iso}(H) = 1.2U_{eq}(C)$ ($U_{iso}(H) = 1.5U_{eq}(C)$ for CH_3-groups). The calculations were performed using the SHELX-2014 program package [65]. CCDC-1879328 contains the supplementary crystallographic data for this paper. These data can also be obtained free of charge at ccdc.cam.ac.uk/structures (Cambridge Crystallographic Data Centre).

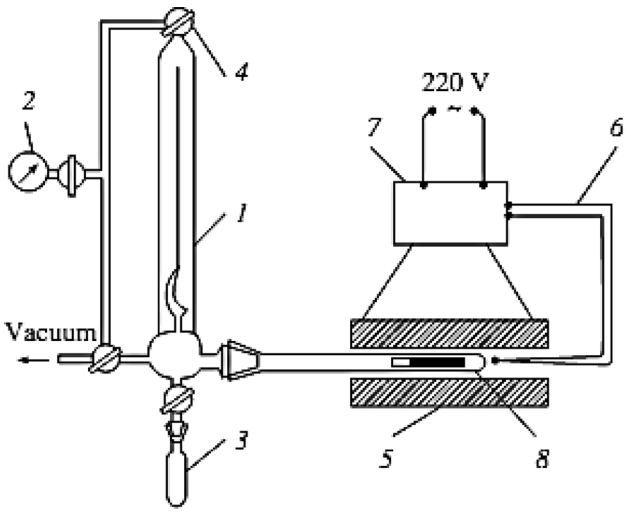

Fig. 1 The scheme of a unit for kinetic studies of the thermolysis of complex **1**: (1) reaction vessel, (2) vacuum gauge, (3) vessel for sampling of gaseous products, (4) vacuum cock, (5) furnace for calcination, (6) thermocouple, (7) heat controller, and (8) ampule with substance

3 Results and Discussion

Complex **1** was synthesized by the reaction of an excess of **L** with the initial nickel maleate in ethanol. Complex **1** is a green crystalline substance, easily soluble in ethanol. According to the elemental analysis, the complex can be formulated as [Ni(Mal)(L)]. The IR spectrum fits well with coordination architectures of related complexes obtained previously [54, 55].

The solid-state structure of complex **1** was determined by single-crystal X-ray diffraction. The crystal and structure refinement data of the compound are given in Table 1.

X-ray crystal analysis shows that the compound is a 1D coordination polymer formed from a 4′-phenyl-terpyridine-Ni(II) node bridged by maleate ligands and crystallizes in monoclinic form with space group $P2_1/n$. There are two Ni(II) moiety's in the asymmetric unit. Each nickel atom is five coordination and is chelated by three nitrogen atoms of **L** and two oxygen atoms of Mal fragments with the formation of a NiN_3O_2 chelate node (Fig. 2).

The complex structure is described in detail. The selected bond lengths and angels of the complex are listed in Table 2.

Nickel five-coordination complexes are common in the coordination chemistry of terpyridine derivatives [56–59]. Five coordinate complexes with chelating ligands can have either a square pyramidal or trigonal bipyramidal geometry, and both steric and electronic factors influence the specific case. The change in the five coordinate species between the square pyramidal and trigonal bipyramidal is quantified using Reedijk's τ values calculated by the formula (2):

$$\tau = (\beta - \alpha)/60, \quad (2)$$

where β is the largest X–Ni–X bond angle and α is the second largest X–Ni–X angle [60].

The coordination polyhedrons of two Ni(II) moiety's in complex **1** are closer to the square pyramidal than to the trigonal bipyramidal, because the values of the Reedijk's τ parameter are closer to 0 (the ideal tetragonal pyramid) than

Table 1 Crystallographic data and structures refinement details for complex **1**

Empirical formula	$C_{50}H_{34}N_6Ni_2O_8$	
M_r	964.25	
Temperature	120.0 K	
Wavelength	0.71073 Å	
Crystal system	Monoclinic	
Space group	$P2_1/n$	
Unit cell dimensions	a = 13.493(5) Å	α = 90°
	b = 18.411(7) Å	β = 98.832(9)°
	c = 16.239(6) Å	γ = 90°
Volume	3986(3) $Å^3$	
Z	4	
Density (calculated)	1.607 Mg/m^3	
Absorption coefficient	1.015 mm^{-1}	
F(000)	1984	
Crystal size	0.14 × 0.09 × 0.03 mm^3	
Theta range for data collection	1.683° to 25.998°	
Index ranges	$-16 \le h \le 16, -22 \le k \le 22, -20 \le l \le 20$	
Reflections collected	38,056	
Independent reflections	7823 [R(int) = 0.1721]	
Completeness to theta = 25.242°	100.0%	
Absorption correction	Semi-empirical from equivalents	
Max. and min. transmission	0.7459 and 0.6402	
Refinement method	Full-matrix least-squares on F^2	
Data/restraints/parameters	7823/0/595	
Goodness-of-fit on F^2	0.963	
Final R indices [I > 2sigma(I)]	R1 = 0.0566, wR2 = 0.1118	
R indices (all data)	R1 = 0.1386, wR2 = 0.1464	
Extinction coefficient	n/a	
Largest diff. peak and hole	0.771 and −0.617 e $Å^{-3}$	

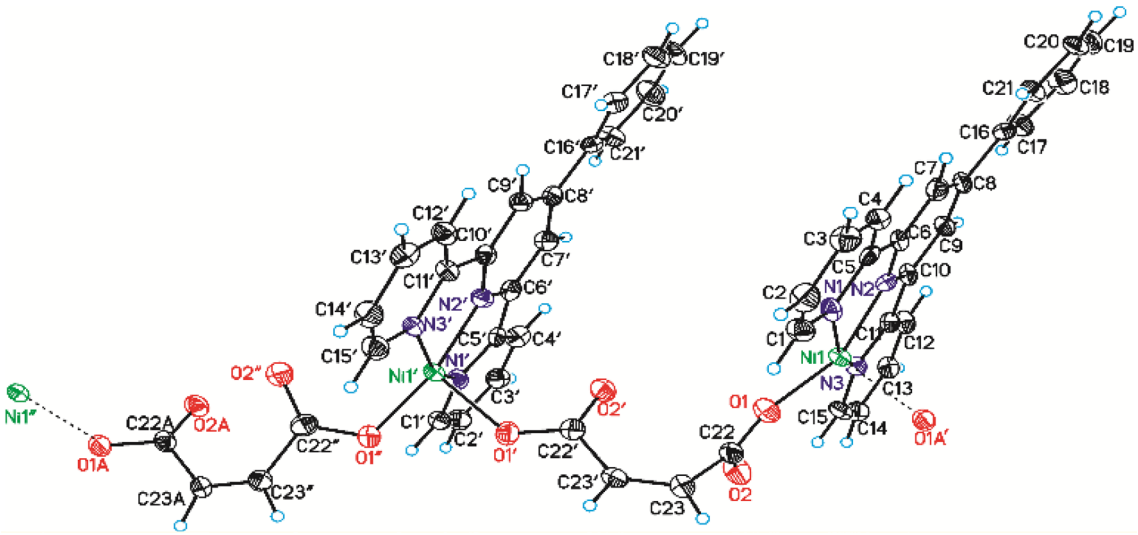

Fig. 2 Molecular structure of complex **1** including the atom numbering scheme. The labeling for all hydrogen atoms has been omitted for clarity

Table 2 Selected bond lengths and angles for the complex **1**

Bond	d/Å	Bond	d/Å	Bond	d/Å
Ni(1)–O(1)	1.924(4)	Ni(1)–O(1A)$^{\#1}$	2.135(4)	Ni(1)–N(1)	2.077(4)
Ni(1)–N(2)	1.939(4)	Ni(1)–N(3)	2.069(4)	Ni(1′)–O(1′)	2.141(4)
Ni(1′)–O(1″)	1.913(4)	Ni(1′)–N(1′)	2.049(4)	Ni(1′)–N(2′)	1.941(4)
Ni(1′)–N(3′)	2.067(4)	O(1A)–Ni(1)$^{\#2}$	2.135(4)	C(22A)–O(1A)	1.277(6)
C(2)–C(1)	1.374(7)	N(1)–C(1)	1.330(6)	C(22A)–C(23A)	1.492(7)
Angle	ω/deg	Angle	ω/deg	Angle	ω/deg
N(3′)–Ni(1′)–O(1′)	94.22(16)	N(1′)–Ni(1′)–O(1′)	101.42(15)	N(1′)–Ni(1′)–N(3′)	155.74(18)
O(1″)–Ni(1′)–O(1′)	87.95(15)	O(1″)–Ni(1′)–N(3′)	103.37(16)	O(1″)–Ni(1′)–N(1′)	95.67(17)
O(1″)–Ni(1′)–N(2′)	165.48(17)	N(2′)–Ni(1′)–O(1′)	106.35(16)	N(2′)–Ni(1′)–N(3′)	78.51(17)
N(2′)–Ni(1′)–N(1′)	79.35(18)	N(2)–Ni(1)–O(1A)$^{\#1}$	102.44(16)	N(2)–Ni(1)–N(1)	78.20(18)
N(2)–Ni(1)–N(3)	79.24(17)	N(1)–Ni(1)–O(1A)$^{\#1}$	91.25(16)	N(3)–Ni(1)–O(1A)$^{\#1}$	100.34(16)
N(3)–Ni(1)–N(1)	156.38(18)	O(1)–Ni(1)–N(2)	158.68(17)	O(1)–Ni(1)–O(1A)$^{\#1}$	94.63(16)
O(1)–Ni(1)–N(1)	88.85(16)	O(1)–Ni(1)–N(3)	110.40(16)	C(22A)–O(1A)–Ni(1)$^{\#2}$	123.1(3)
C(10)–N(2)–Ni(1)	119.5(4)	C(5)–N(1)–Ni(1)	114.4(3)	C(6)–N(2)–Ni(1)	120.1(4)
C(1)–N(1)–Ni(1)	126.8(4)	C(11)–N(3)–Ni(1)	113.7(3)	C(15)–N(3)–Ni(1)	128.3(4)

Symmetry transformations used to generate equivalent atoms

$^{\#1}$x,y,z + 1

$^{\#2}$x,y,z − 1

1 (the trigonal bipyramid). At the same time, the polyhedron of the Ni(1) moiety is close to the ideal tetragonal pyramidal structure ($\tau = 0.038$), while the polyhedron of the Ni(1′) moiety belongs to the distorted tetragonal pyramidal structure ($\tau = 0.162$). Base planes are created by the two N atom from the ligand, N1 and N3, and by two oxygen atoms from the Mal ligands. The remaining N2 atom of ligand molecule is at the apex position. The lengths of the bonds Ni(1)–N(1) (2.077 Å), Ni(1)–N(2) (1.939 Å), and Ni(1)–N(3) (2.069 Å) are within the normal range of Ni–N bonds for five-coordinate nickel complexes with terpyridine derivatives [56–59]. The rigid nature of the **L** bite forces the lengths of the Ni–N bonds in the complex to follow the general tendency of the Ni–terpyridine complexes, namely, that their central Ni–N bond is slightly shorter than the lateral Ni–N bonds.

It is well known [16] that the conjugated thermolysis of unsaturated metal carboxylates consists of two successive key stages [16]: solid-phase polymerization of the initial monomer and decarboxylation of the resulting metallopolymer, accompanied by intense gas evolution. According to the data of thermal analysis (Fig. 3), the first stage of thermolysis of complex **1** takes place up to 230 °C and is accompanied by a slight weight loss (less than 10%) against the background of a continuously growing exothermic effect from 0.8 to 1.7 mW. At this stage, the structural transformation of the coordination polymer occurs and its solid-phase polymerization proceeds. The second stage includes decarboxylation followed by a deeper decomposition of the polymer, starting at 230 °C, and associated with a short-term significant evolution of gases, reaching a peak at 232 °C against the background of a sharp increase in the endothermic effect. The temperature interval from 230 to 250 °C has a significant weight loss of to 46 wt% of the original sample and is associated not only with decarboxylation, but also with partial elimination of maleic acid and terpyridine ligand, forming a volatile adduct under these conditions. Above 230 °C to 380 °C a significant increase in the exothermic effect is observed from 1.7 to 8 mW against the background of a moderate weight loss of 15.3%.

The first stage of reaction is initiated in accordance with the Borodin–Hunsdiecker mechanism: the initial slight decarboxylation leads to the formation of biradicals $^{\bullet}$OOCCH=CHCOO$^{\bullet}$, which, in turn, cause the polymerization and the formation of polymers (Scheme 1).

The kinetics of isothermal transformations of complex **1** was studied on the basis of the evolution of gas in a static non-isothermal reactor using a manometer with a zero membrane. To measure the volume of gaseous products released, the temperature range is determined at which, according to the TG data coupled to the mass spectrometer, there is an intense release of gaseous products. In the future, the sample of the substance is heated and the released gas determine volumetrically in the specified interval.

We have previously shown [26] that the kinetics of the evolution of the gas $\eta(\tau)$ in the general case (up $\eta \leq 0.95$) is satisfactorily approximated by the equation for the two parallel reactions:

$$\eta(\tau) = \eta_{1f}\left[1-\exp(-k_1\tau)\right] + \left(1-\eta_{1f}\right)\left[1-\exp(-k_2\tau)\right] \quad (3)$$

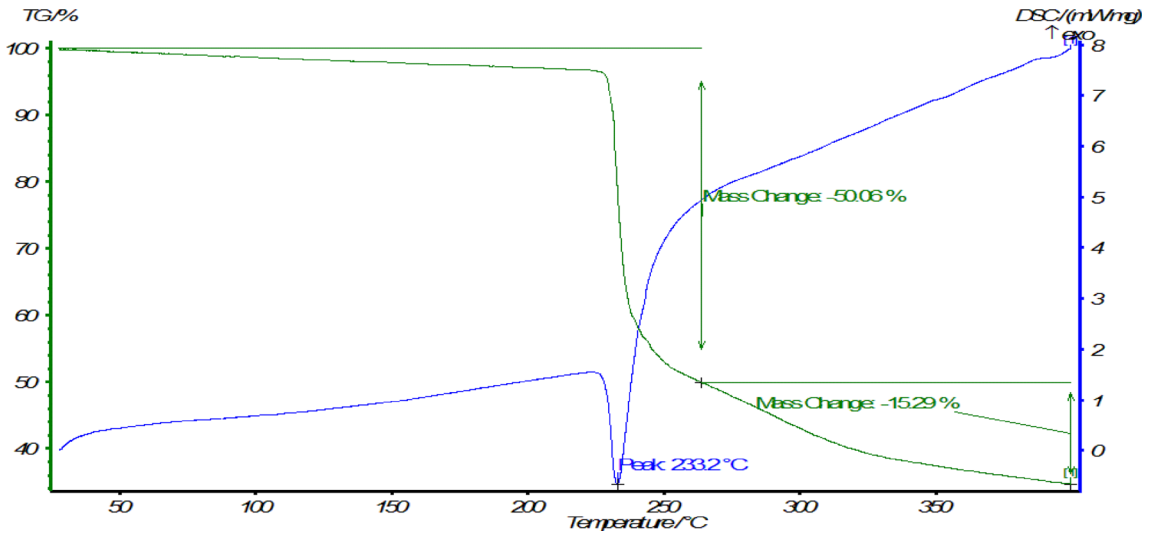

Fig. 3 Thermogram of the complex **1**

I. Initiation

$$n\,[Ni(OOCCH=CHCOO)L] \xrightarrow[-[Ni(OOCCH=CHCOO)L]_{n-1}]{} (^{\bullet}OOCCH=CHCOO^{\bullet}) + L$$

$$\underbrace{(^{\bullet}OOCCH=CHCOO^{\bullet}) + 2[Ni(OOCCH=CHCOO)L] \rightarrow HOOCCH=CHCOOH + Ni(OOC^{\bullet}C=CHCOO)L}_{R^{\bullet}}$$

II. Polymerization

$$R^{\bullet} + n\,[Ni(OOCCH=CHCOO)L] \rightarrow$$

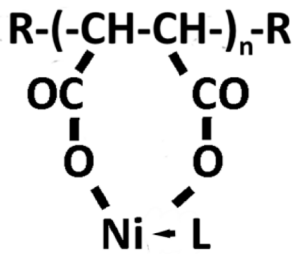

Scheme 1 Scheme of second stage of conjugated thermolysis of complex 1

where η is degree of conversion, $\tau = t - t_0$ (t_0 is the time of heating), $\eta_{1f} = \eta(\tau)|_{k_2 t\to 0,\, k_1 t\to\infty}$, k_1, k_2 are the effective rate constants.

The initial rate of gas evolution $W_{\tau=0} = W_0$ is

$$W_0 = \eta_{1f} k_1 + (1-\eta_{1f}) k_2 \quad (4)$$

Equations (3) and (4) describe the kinetics of the gas evolution of complex **1** and the dependence of the logarithm of the thermolysis rate constant on inverse temperature for complex **1** are shown in Fig. 4. Analytically calculated activation energy of conjugated thermolysis is $E_a = 589$ kJ/mol.

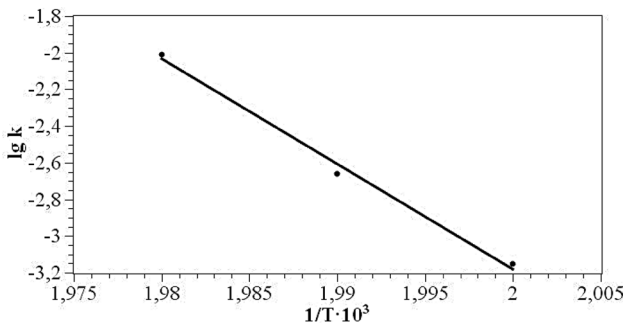

Fig. 4 Dependence lg*k* versus 1/T for complex **1**

The powder obtained at the end of thermolysis of complex **1** is a shiny powder of black color, which is explained by the presence of amorphous carbon [13]. The product obtained by thermolysis of complex **1** was investigated by X-ray diffraction analysis, which made it possible to obtain data on its phase composition and crystallite size (Fig. 5). XRD pattern of the powder of the thermolysis products of complex **1** at 300 °C in a self-generated atmosphere suggests that the nickel nanoparticles are included in the matrix of an amorphous polymer, giving clear diffraction peaks located in the region of 2Θ of 44.45 and 51.75. The data on the structure of **fcc** β-Ni phase were taken from the JCPDC database (nos. 04-0850) [61]. The calculation using the Debye–Scherrer formula allowed us to determine the size of crystallites of 22.08 nm (for a reflection angle of 2Θ = 44.45) and 55.05 nm (for a reflection angle of 2Θ = 51.75), the average crystallite size is 38.57 nm.

The absence of the ν(C=C) and δ(=CH) absorption bands at 1644 and 1106 cm^{-1} confirms the consumption of C=C bonds as a result of polymerization (Fig. 6). The IR data lead us to conclude that, during the thermolysis, the initial structure of the formed metallopolymer undergoes degradation, with some fragments remaining preserved. Broad absorption bands arise in the region of 1600 cm^{-1}, which attest to the presence of the stretching vibrations of C–C bonds typical of triene and diene conjugated fragments. The band at 1560 cm^{-1} relates to the stretching vibrations of the N-heterocycle. All absorption bands have a Gaussian pattern, showing that interatomic and deformational vibrations occur in a limited space and the system is characterized by a high degree of crosslinking.

Considering our previous data [2–4, 14, 62] and based on IR spectroscopy and elemental analysis (N, 7.21%; Ni, 16.1%; C, 58.9%), it is assumed the formation of a network containing conjugated double bonds and C=N fragments.

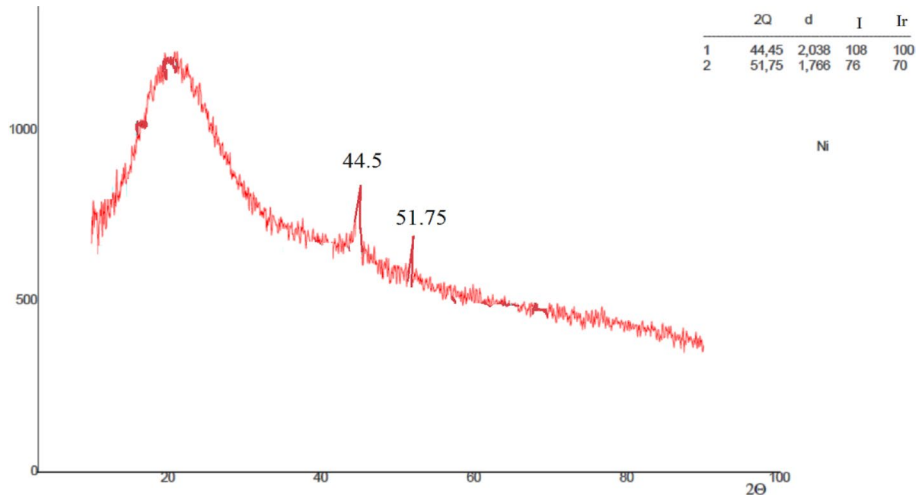

Fig. 5 X-ray diffraction pattern of the thermolysis product of complex **1** in a self-generated atmosphere

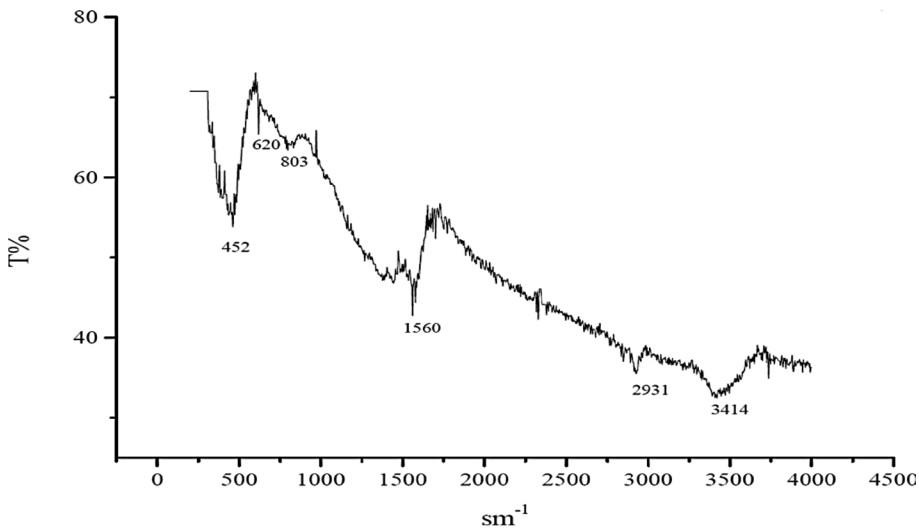

Fig. 6 IR spectrum of the product of thermolysis of complex **1** at 300 °C in a self-generated atmosphere

According to high-resolution transmission electron microscopy (HRTEM) data (Fig. 7), the obtained nanoparticles have a spherical shape with an average size of 28 nm. At the same time, the products of nickel maleate thermolysis were agglomerated with an average size of 5.5–20.5 μm [3], which indicates the effect of chelating N-heterocycle on the structure and size of the products of conjugated thermolysis. From the HRTEM data it is clearly seen that there are electron-dense metallic particles in electron-less-dense polymeric matrix.

The combination of experimental data allows us to conclude that nanoparticles in such a system have a characteristic "core–shell" structure, which includes a metal-containing core and a polymer shell (Scheme 2). It should be noted that nanoparticles of metals with a "core–shell" structure have recently been the subject of numerous studies, and first of all, attention to them is due to the possibility of combining various properties (magnetic, electrical, optical) in one nanoparticle by changing the composition and number of layers [16, 63]. Conjugated thermolysis of unsaturated metal carboxylates makes it possible to obtain metal–polymer core–shell nanocomposites in one stage. A distinctive feature is their stability over time; no changes are observed in the chemical composition, size and shape of nanoparticles during their storage.

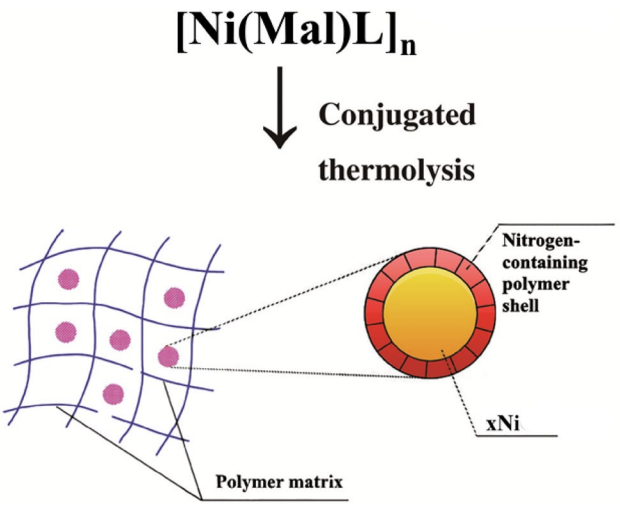

Scheme 2 Scheme of formation of core-shell nanoparticles

4 Conclusion

In this article, we report the synthesis and structural characterization of a new complex based on nickel(II) maleate and 4′-phenyl-2,2′:6′,2″-terpyridine. We found that this complex is a 1D coordination polymer containing two five-coordinated Ni(II) moiety's in the asymmetric unit. In addition, the metal chelate node has the ideal tetragonal pyramidal geometry for the first Ni(II) moiety and the distorted tetragonal pyramidal structure for the second Ni(II) moiety. Conjugated thermolysis of complex **1** made it possible to obtain a

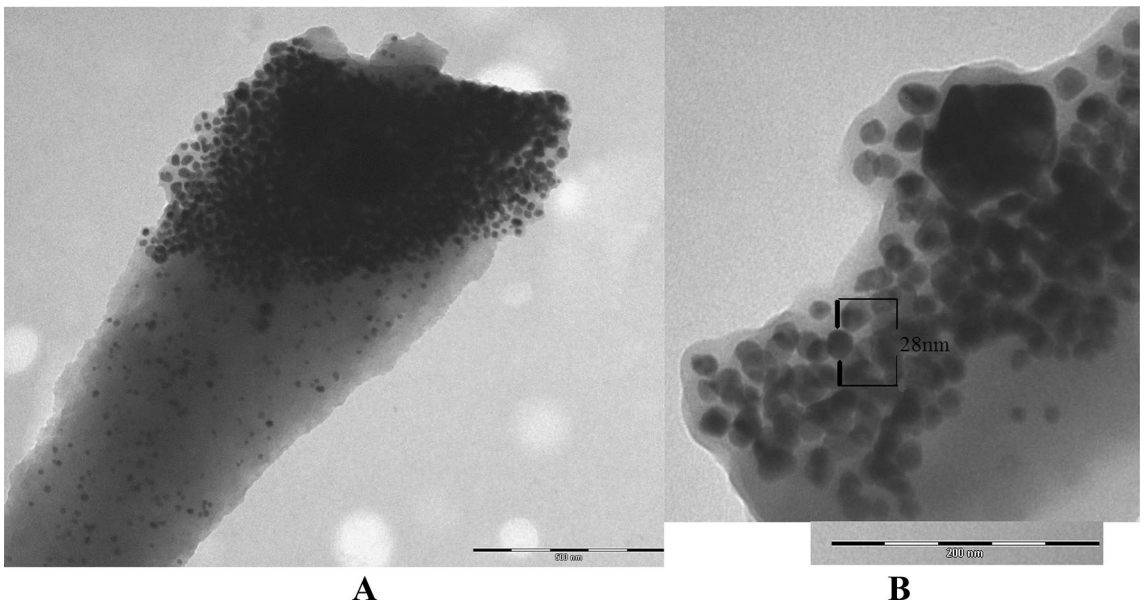

Fig. 7 HRTEM image of the morphology of the product of thermolysis of complex **1**: ×43,000 (**a**), ×105,000 (**b**)

metal-polymer nanocomposite containing metal nanoparticles uniformly distributed in a stabilizing nitrogen-containing polymer matrix. We believe that such nanocomposite materials can be used further, for example, as anti-friction additives to lubricants, which is the subject of our further research.

Acknowledgements We are grateful to Dr. Kyrill Y. Suponitsky (A.N. Nesmeyanov Institute of Organoelement Compounds, Moscow) for X-ray study.

References

1. G.I. Dzhardimalieva, I.E. Uflyand, Design and synthesis of coordination polymers with chelated units and their application in nanomaterials science. RSC Adv. **7**, 42242–42288 (2017)
2. A.D. Pomogailo, G.I. Dzhardimalieva, A.S. Rozenberg, D.M. Muraviev, Kinetics and mechanism of in situ simultaneous formation of metal nanoparticles in stabilizing polymer matrix. J. Nanopart. Res. **5**, 497–519 (2003)
3. VYu. Musatova, S.A. Semenov, D.V. Drobot, A.S. Pronin, A.D. Pomogailo, G.I. Dzhardimalieva, V.I. Popenko, Synthesis and thermal conversions of unsaturated nickel(II) dicarboxylates as precursors of metallopolymer nanocomposites. Russ. J. Inorg. Chem. **61**, 1111–1124 (2016)
4. S.A. Semenov, VYu. Musatova, D.V. Drobot, G.I. Dzhardimalieva, Thermal decomposition of unsaturated nickel(II) dicarboxylates. Russ. J. Inorg. Chem. **63**, 1217–1224 (2018)
5. M. Padmanabhan, J.C. Joseph, A. Thirumurugan, C.N.R. Rao, Maleate–fumarate conversion and other novel aspects of the reaction of a Co(II) maleate with pyridine and bipyridine. Dalton Trans. **21**, 2809–2811 (2008)
6. J.-M. Yang, Z.-H. Zhou, H. Zhang, H.-L. Wan, S.-J. Lu, Temperature effect on the conversions of phthalato and maleato manganese(II) complexes with diamine ligands. Inorg. Chim. Acta **358**, 1841–1849 (2005)
7. L.I. Yudanova, V.A. Logvinenko, N.F. Yudanov, N.A. Rudina, A.V. Ishchenko, P.P. Semyannikov, L.A. Sheludyakova, N.I. Alferova, Thermolysis of copper(II) salts of maleic acid. Synthesis of metal–polymer composites. Russ. J. Coord. Chem. **39**, 415–420 (2013)
8. L.I. Yudanova, V.A. Logvinenko, L.A. Sheludyakova, N.F. Yudanov, P.P. Semyannikov, S.I. Kozhemyachenko, I.V. Korolkov, N.A. Rudina, A.V. Ishchenko, Maleates of Mn(II), Fe(II), Co(II), and Ni(II) as precursors for synthesis of metal-polymer composites. Russ. J. Inorg. Chem. **59**, 1180–1186 (2014)
9. V.A. Logvinenko, L.I. Yudanova, N.F. Yudanov, G.N. Chekhova, Thermal analysis of transition metal salts of carboxylic acids. The way for the synthesis of metal–polymer composites. J. Therm. Anal. Calorim. **74**, 395–399 (2003)
10. L.I. Yudanova, V.A. Logvinenko, L.A. Sheludyakova, I.V. Korolkov, A.V. Ishchenko, N.A. Rudina, Regularities of thermolysis for the Fe(II), Co(II), and Ni(II) salts of maleic and *ortho*-phthalic acids with the formation of metal/polymer composites. Russ. J. Coord. Chem. **43**, 446–452 (2017)
11. A.K. Nikumbh, S.K. Pardeshi, M.N. Raste, A study of the thermal decomposition of copper(II) and zinc(II) malonate, maleate and succinate complexes using direct current electrical conductivity measurements. Thermochim. Acta **374**, 115–128 (2001)
12. N.-Q. Bui, C. Geantetand, G. Berhault, Activation of regenerated $CoMo/Al_2O_3$ hydrotreating catalysts by organic additives—The particular case of maleic acid. Appl. Catal. A **572**, 185–196 (2019)
13. L.I. Yudanova, V.A. Logvinenko, N.F. Yudanov, N.A. Rudina, A.V. Ishchenko, P.P. Semyannikov, L.A. Sheludyakova, N.I. Alferova, A.I. Romanenko, O.B. Anikeev, Preparation of metal–polymer composites through the thermolysis of Fe(II), Co(II), and Ni(II) maleates. Inorg. Mater. **49**, 1055–1060 (2013)
14. N.P. Porolo, Z.G. Aliev, G.I. Dzhardimalieva, I.N. Ivleva, I.E. Uflyand, A.D. Pomogailo, N.S. Ovanesyan, Synthesis and reactivity of metal-containing monomers. Synthesis and structure of salts of unsaturated dicarboxylic acids. Russ. Chem. Bull. **46**, 362–370 (1997)
15. L.I. Yudanova, V.A. Logvinenko, L.A. Sheludyakova, N.F. Yudanov, G.N. Chekhova, N.I. Alferova, V.I. Alekseev, P.P. Semyannikov, V.I. Lisoivan, Thermal decomposition of solid solutions in systems of Fe(II), Co(II), and Ni(II) hydrogen maleates with the formation of bimetallic nanoparticles. Russ. J. Inorg. Chem. **53**, 1459 (2008)
16. I.E. Uflyand, G.I. Dzhardimalieva, *Nanomaterials Preparation by Thermolysis of Metal Chelates* (Springer, Cham, 2018)
17. S.A. Semenov, VYu. Musatova, D.V. Drobot, G.I. Dzhardimalieva, Quantitative description of properties of nickel-containing nanocomposites affecting their magnetic characteristics. Russ. J. Inorg. Chem. **63**, 1424–1426 (2018)
18. M. Badea, R. Olar, D. Marinescu, G. Vasile, Some new acrylate complexes as a criterion in their selection for further co-polymerization reaction. J. Therm. Anal. Calorim. **80**, 683–685 (2005)
19. C.-B. Liu, M.-X. Yu, X.-J. Zheng, L.-P. Jin, S. Gao, S.-Z. Lu, Structural change of supramolecular coordination polymers of itaconic acid and 1,10-phenanthroline along lanthanide series. Inorg. Chim. Acta **358**, 2687–2696 (2005)
20. G.V. Scaeteanu, M.C. Chifiriuc, C. Bleotu, C. Kamerzan, L. Marutescu, C.G. Daniliuc, C. Maxim, L. Calu, R. Olar, M. Badea, Synthesis, structural characterization, antimicrobial activity, and in vitro biocompatibility of new unsaturated carboxylate complexes with 2,2′-bipyridine. Molecules **23**, 157 (2018)
21. A. Uhrinová, J. Kuchár, A. Orendáčová, M. Pitoňák, J. Federič, J. Noga, J. Černá, $[Ni(bpy)(mal)(H_2O)_3]\cdot H_2O$ and $[Ni(4,4'\text{-dmbpy})(mal)(H_2O)_3]\cdot 1.5H_2O$: syntheses, crystal structures, magnetic properties, and computational study of stacking interactions. J. Coord. Chem. **70**, 2999–3018 (2017)
22. A. Pavlová, J. Černák, K. Harm, Bis(2,2′-bipyridine-k^2N,N')(maleate-$k^2O^1,O^{1'}$)nickel(II) 7.34-hydrate. Acta Crystallogr. Sect. E **64**, m1536–m1537 (2008)
23. M. Li, X. Fu, C. Wang, Tri-aqua-(2,2′-bi-pyridine) maleatonickel(II) monohydrate. Acta Crystallogr. Sect. E **62**, m865–m866 (2006)
24. L. Wiehl, J. Schreuer, E. Haussühl, Crystal structure of tri-aqua-1,10-phenanthroline-nickel(II) maleate dihydrate, $Ni(H_2O)_3(C_{12}H_8N_2)(C_4H_2O_4)\cdot 2H_2O$. Z. Kristallogr. - New Cryst. Struct. **223**, 82–84 (2008)
25. Y.-Q. Zheng, J.-L. Lin, Z.-P. Kong, B.-Y. Chen, Self-assemblies of Ni(II) with phenanthroline and maleate anions: $[Ni(H_2O)_3(phen)L].H_2O$ (1) and $[Ni(H_2O)_2(phen)L].2H_2O$ (2) with H_2L = maleic acid. J. Chem. Crystallogr. **32**, 399–408 (2002)
26. I.E. Uflyand, V.A. Zhinzhilo, L.S. Lapshina, A.A. Novikova, V.E. Burlakova, G.I. Dzhardimalieva, Conjugated thermolysis of metal chelate monomers based on cobalt acrylate complexes with polypyridyl ligands and tribological performance of nanomaterials obtained. ChemistrySelect **3**, 8998–9007 (2018)
27. H.-H. Zou, L. Wang, Z.-X. Long, Q.-P. Qin, Z.-K. Song, T. Xie, S.-H. Zhang, Y.-C. Liu, B. Lin, Z.-F. Chen, Preparation of 4-([2,2′:6′,2″-terpyridin]-4′-yl)-N, *N*-diethylaniline NiII and PtII complexes and exploration of their in vitro cytotoxic activities. Eur. J. Med. Chem. **108**, 1–12 (2016)

28. E.C. Constable, J. Lewis, M.C. Liptrot, P.R. Raithby, The coordination chemistry of 4′-phenyl-2,2′:6′,2″-terpyridine; the synthesis, crystal and molecular structures of 4′-phenyl-2,2′:6′,2″-terpyridine and bis(4′-phenyl-2,2′:6′,2″-terpyridine)nickel(II) chloride decahydrate. Inorg. Chim. Acta **178**, 47–54 (1990)
29. W.-W. Fu, Y.-Q. Li, Y. Liu, M.-S. Chen, W. Li, Y.-Q. Yang, An infinite two-dimensional hybrid water–chloride network in a 4′-(furan-2-yl)-2,2′:6′,2″-terpyridine nickel(II) matrix. Acta Cryst. E **73**, 871–875 (2017)
30. W.-W. Fu, D.-Z. Kuang, F.-X. Zhang, Y. Liu, W. Li, Y.-F. Kuang, Synthesis, crystal structure and properties of the nickel(II) 4′-(p-methoxy1pheny1)-2, 2′:6′,2″-terpyridine complex. Chin. J. Inorg. Chem. **29**, 654–658 (2013)
31. J. McMurtrie, I. Dance, Crystal packing in metal complexes of 4′-phenylterpyridine and related ligands: occurrence of the 2D and 1D terpy embrace arrays. CrystEngComm **11**, 1141–1149 (2009)
32. W.-W. Fu, X. Shu, Y.-L. Luo, Z.-Q. Tang, Q. Li, H.-J. Liu, Q.-W. Cheng, H.-Y. Wang, Y. Liu, New Co(II) and Mn(II) complexes with 4′-substituted 2,2′:6′,2″-terpyridine ligands. J. Struct. Chem. **59**, 398–410 (2018)
33. Y.H. Lee, E. Kubota, A. Fuyuhiro, S. Kawata, J.M. Harrowfield, Y. Kim, S. Hayami, Synthesis, structure and luminescence properties of Cu(II), Zn(II) and Cd(II) complexes with 4′-terphenylterpyridine. Dalton Trans. **41**, 10825–10831 (2012)
34. B.N. Ghosh, F. Topić, P.K. Sahoo, P. Mal, J. Linnera, E. Kalenius, H.M. Tuononen, K. Rissanen, Synthesis, structure and photophysical properties of a highly luminescent terpyridine-diphenylacetylene hybrid fluorophore and its metal complexes. Dalton Trans. **44**, 254–267 (2015)
35. S. Naik, S. Kumar, J.T. Mague, M.S. Balakrishna, A hybrid terpyridine-based bis(diphenylphosphino)amine ligand, terpy-$C_6H_4N(PPh_2)_2$: synthesis, coordination chemistry and photoluminescence studies. Dalton Trans. **45**, 18434–18437 (2016)
36. W.-W. Fu, F.-X. Zhang, D.-Z. Kuang, Y. Liu, Y.-Q. Yang, Syntheses, crystal structures and luminescence of zinc(II) and cadmium(II) complexes with 4′-substituted 2,2′:6′,2″-terpyridines. J. Coord. Chem. **68**, 1177–1188 (2015)
37. W.-W. Fu, Q. Huang, S.T. Liu, W.J. Wu, J.R. Shen, S.H. Li, Syntheses, crystal structures, and luminescence properties of Co(II), Ni(II) and Zn(II) complexes with 4′-(4-(Imidazol-1-Yl)phenyl)-2,2′:6′,2″-terpyridine. Russ. J. Coord. Chem. **43**, 670–678 (2017)
38. Y. Komatsu, K. Kato, Y. Yamamoto, H. Kamihata, Y.H. Lee, A. Fuyuhiro, S. Kawata, Spin-crossover behaviors based on intermolecular interactions for cobalt(II) complexes with long alkyl chains. Eur. J. Inorg. Chem. **2012**, 2769–2775 (2012)
39. Y. Zhang, K.L.M. Harriman, G. Brunet, A. Pialat, B. Gabidullin, M. Murugesu, Reversible redox, spin crossover, and superexchange coupling in 3d transition-metal complexes of bis-azinyl analogues of 2,2′:6′,2″-terpyridine. Eur. J. Inorg. Chem. **2018**, 1212–1223 (2018)
40. M. Nakaya, R. Ohtani, J.W. Shin, M. Nakamura, L.F. Lindoy, S. Hayami, Abrupt spin transition in a modified-terpyridine cobalt(II) complex with a highly-distorted $[CoN_6]$ core. Dalton Trans. **47**, 13809–13814 (2018)
41. W.W. Fu, M.S. Chen, W. Li, Y. Liu, F.X. Zhang, D.Z. Kuang, Hydrothermal syntheses, crystal structures, and magnetic properties of three manganese(II) complexes based on 4′-substituted 2,2′:6′,2″-terpyridine ligands. Russ. J. Coord. Chem. **41**, 247–254 (2015)
42. V.D. Singh, R.S. Singh, R.P. Paitandi, B.K. Dwivedi, B. Maiti, D.S. Pandey, Solvent-dependent self-assembly and aggregation-induced emission in Zn(II) complexes containing phenothiazine-based terpyridine ligand and its efficacy in pyrophosphate sensing. J. Phys. Chem. C **122**, 5178–5187 (2018)
43. A. Sil, A. Maity, D. Giri, S.K. Patra, A phenylene–vinylene terpyridine conjugate fluorescent probe for distinguishing Cd^{2+} from Zn^{2+} with high sensitivity and selectivity. Sens. Actuators B **226**, 403–411 (2016)
44. K. Czerwińska, B. Machura, S. Kula, S. Krompiec, K. Erfurt, C. Roma-Rodrigues, A.R. Fernandes, L.S. Shulpina, N.S. Ikonnikov, G.B. Shulpin, Copper(II) complexes of functionalized 2,2′:6′,2″-terpyridines and 2,6-di(thiazol-2-yl)pyridine: structure, spectroscopy, cytotoxicity and catalytic activity. Dalton Trans. **46**, 9591–9604 (2017)
45. Z. Ma, L. Wei, E.C.B.A. Alegria, L.M.D.R.S. Martins, M.F.C. Guedes, A.J.L. Pombeiro, Synthesis and characterization of copper(II) 4′-phenyl-terpyridine compounds and catalytic application for aerobic oxidation of benzylic alcohols. Dalton Trans. **43**, 4048–4058 (2014)
46. Y.H. Budnikova, D.A. Vicic, A. Klein, Exploring mechanisms in Ni terpyridine catalyzed C–C cross-coupling reactions—a review. Inorganics **6**, 18 (2018)
47. D. Zych, A. Slodek, M. Matussek, M. Filapek, G. Szafraniec-Gorol, S. Krompiec, S. Kotowicz, M. Siwy, E. Schab-Balcerzak, K. Bednarczyk, M. Libera, K. Smolarek, S. Maćkowski, W. Danikiewicz, Highly luminescent 4′-(4-ethynylphenyl)-2,2′:6′,2″-terpyridine derivatives as materials for potential applications in organic light emitting diodes. ChemistrySelect **2**, 8221–8233 (2017)
48. A. Sil, S.R. Chowdhury, S. Mishra, S.K. Patra, Synthesis, structure, and photophysical and electrochemical properties of Ru(II) complexes of arylene–vinylene terpyridyl conjugates. Dalton Trans. **47**, 9877–9888 (2018)
49. U.S. Schubert, H. Hofmeier, G.R. Newkome, *Modern Terpyridine Chemistry* (Wiley, Weinheim, 2006)
50. Y.-W. Zhong, C.-J. Yao, H.-J. Nie, Electropolymerized films of vinyl-substituted polypyridine complexes: synthesis, characterization, and applications. Coord. Chem. Rev. **257**, 1357–1372 (2013)
51. G.I. Dzhardimalieva, I.E. Uflyand, Review: recent advances in the chemistry of metal chelate monomers. J. Coord. Chem. **70**, 1468–1527 (2017)
52. G.I. Dzhardimalieva, I.E. Uflyand, Metal chelate monomers as precursors of polymeric materials. J. Inorg. Organomet. Polym Mater. **26**, 1112–1173 (2016)
53. G.I. Dzhardimalieva, I.E. Uflyand, *Chemistry of Polymeric Metal Chelates* (Springer, Cham, 2018)
54. M. Wałęsa-Chorab, A.R. Stefankiewicz, A. Gorczyński, M. Kubicki, J. Kłak, M.J. Korabik, V. Patroniak, Structural, spectroscopic and magnetic properties of new copper(II) complexes with a terpyridine ligand. Polyhedron **30**, 233–240 (2011)
55. M. Wałęsa-Chorab, A.R. Stefankiewicz, D. Ciesielski, Z. Hnatejko, M. Kubicki, J. Kłak, M.J. Korabik, V. Patroniak, New mononuclear manganese(II) and zinc(II) complexes with a terpyridine ligand: structural, magnetic and spectroscopic properties. Polyhedron **30**, 730–737 (2011)
56. A. Gorczyński, M. Wałęsa-Chorab, M. Kubicki, M. Korabik, V. Patroniak, New complexes of 6,6″-dimethyl-2,2′:6′,2″-terpyridine with Ni(II) ions: synthesis, structure and magnetic properties. Polyhedron **77**, 17–23 (2014)
57. W.-W. Fu, J.-R. Shen, Z.-Q. Tang, Y.-Q. Peng, Q. Yi, Synthesis, crystal structure and magnetic property of a Ni(II) complex with 4′-(4-methoxyphenyl)-2,2′:6′,2″-terpyridine. Inorg. Nano-Met. Chem. **47**, 1664–1667 (2017)
58. C.-P. Zhang, H. Wang, A. Klein, C. Biewer, K. Stirnat, Y. Yamaguchi, L. Xu, V. Gomez-Benitez, D.A. Vicic, A five-coordinate nickel(II) fluoroalkyl complex as a precursor to a spectroscopically detectable Ni(III) species. J. Am. Chem. Soc. **135**, 8141–8144 (2013)
59. E.C. Constable, D. Phillips, P.R. Raithby, Nickel(II) chloride adducts of 4′-phenyl-2,2′:6′,2″-terpyridine. Inorg. Chem. Commun. **5**, 519–521 (2002)

60. A.W. Addison, T.N. Rao, J. Reedijk, J. Van Rijn, G.C. Verschoor, Synthesis, structure, and spectroscopic properties of copper(II) compounds containing nitrogen–sulphur donor ligands; the crystal and molecular structure of aqua[1,7-bis(N-methylbenzimidazol-2′-yl)-2,6-dithiaheptane]copper(II) perchlorate. J. Chem. Soc. Dalton Trans. **7**, 1349–1356 (1984)
61. Y.T. Jeon, J.Y. Moon, G.H. Lee, J. Park, Y. Chang, Comparison of the magnetic properties of metastable hexagonal close-packed Ni nanoparticles with those of the stable face-centered cubic Ni nanoparticles. J. Phys. Chem. B **110**, 1187–1191 (2006)
62. A.D. Pomogailo, G.I. Dzhardimalieva, Controlled thermolysis of macromolecule-metal complexes as a way for synthesis of nanocomposites. Macromol. Symp. **317–318**, 198–205 (2012)
63. R.G. Chaudhuri, S. Paria, Core/shell nanoparticles. Chem. Rev. **112**, 2373–2433 (2012)
64. G.M. Sheldrick, *SADABS. Program for Scanning and Correction of Area Detector Data* (University of Göttingen, Germany, 2004)
65. G.M. Sheldrick, *SHELXT* - Integrated space-group and crystal-structure determination. Acta Crystallogr. Sect. A **71**, 3–8 (2015)